Available online at www.sciencedirect.com
ScienceDirect
Bioelectrochemistry 70 (2007) 287–295
Bioelectrochemistry
www.elsevier.com/locate/bioelechem

In vivo electrical impedance measurements during and after electroporation of rat liver

Antoni Ivorra *, Boris Rubinsky

Department of Bioengineering and Department of Mechanical Engineering, University of California at Berkeley, Berkeley, CA 94720, USA

Received 5 June 2006; received in revised form 3 October 2006; accepted 11 October 2006
Available online 21 October 2006

Abstract

Electroporation is used for *in vivo* gene therapy, drug therapy and minimally invasive tissue ablation. Applying electrical pulses across cells can have a variety of outcomes; from no effect to reversible electroporation to irreversible electroporation. Recently, it has been proposed that measuring the passive electrical properties of electroporated tissues could provide real time feedback on the outcome of the treatment. Here we describe the results from the impedance characterization (single dispersion Cole model) for up to 30 min of the electroporation process in *in vivo* rat livers ($n=8$). The electroporation sequence consisted of 8 pulses of 100 μs with a period of 100 ms. Half of the animals were subjected to field magnitudes considered to have reversible effects (R group, $E=450$ V/cm) whereas for the other half irreversible field amplitudes were applied (I group, $E=1500$ V/cm). As expected, there was an immediate increase of conductivity (R group $\Delta\sigma/\sigma_{t=0}=9\pm3\%$; I group $\Delta\sigma/\sigma_{t=0}=43\pm1\%$). However, the overall long term pattern of change in conductivity after electroporation is complex and different between reversible and irreversible groups. This suggests the superposition of different phenomena which together affect the electrical properties.

Keywords: Electroporation; Electrical impedance; Electrical conductivity; Liver

1. Introduction

Electroporation, or electropermeabilization, is the phenomenon in which cell membrane permeability to ions and macromolecules is increased by exposing the cell to short (microsecond to millisecond) high voltage electric field pulses [1]. While the exact mechanism of permeabilization is not precisely understood experiments show that the application of electrical pulses can have several different effects on the cell membrane, as a function of various pulse parameters; such as amplitude, length, shape, number of repeats and intervals between pulses. As a function of these parameters, the application of the electrical pulse can have no effect, can have a transient permeabilization effect known as reversible electroporation or can cause permanent permeabilization known as irreversible electroporation. Both, reversible and irreversible electroporation have important application in biotechnology and medicine [2]. Reversible electroporation is now commonly used with micro-organisms and cells in culture for transfection and introduction or removal of macromolecules from individual cells. Irreversible electroporation is used for sterilization of liquid media from micro-organisms. During the last decade reversible electroporation has started to be used in living tissues for *in vivo* gene therapy (electrogenetherapy) [3–5] and to enhance the penetration of anti-cancer drugs into undesirable cells (electrochemotherapy) [6]. Recently, irreversible electroporation has also found a use in tissues as a minimally invasive surgical procedure to ablate undesirable tissue without the use of adjuvant drugs [7–9].

Successful electroporation, either reversible or irreversible, depends on too many factors to be reliably applied in an open loop procedure [10,11], in particular when a yield of close to 100% is desired; such as in the treatment of cancer or when rare cells such as oocytes are treated. It is obvious that for optimal application of electroporation it is desirable to be able to close the open loop with feedback information on the outcome of the applied pulse or pulses generated by electropermeabilization systems [12].

A possible method for assessing the effects of electroporation is through measurements of the electrical properties of the

* Corresponding author. Tel./fax: +1 510 643 1866.
E-mail address: antoni.ivorra@gmail.com (A. Ivorra).

1567-5394/$ - see front matter © 2006 Elsevier B.V. All rights reserved.
doi:10.1016/j.bioelechem.2006.10.005

electroporation affected cells or tissues. A simplistic model of a cell can be used to qualitatively understand the effects of electroporation on the cell electrical properties. In such a model, a resistance representing the extra-cellular medium is in parallel with a capacitance accounting for the cell membrane in series with a resistance representing the intra-cellular medium. When electropermeabilization is achieved, then the membrane capacitance is partially shunted by a membrane resistance. Afterwards, resealing of the membrane causes the shunting resistance to increase and the impedance returns to its original values. From these considerations, measuring changes in electrical properties of cells has been proposed for determining the effectiveness of electroporation protocols in individual cells [13,14] and in cell cultures [15]. Similarly changes in electrical properties were proposed for detecting electroporation in tissues [16], including the creation of images of the electroporated tissue volumes by means of Electrical Impedance Tomography [17,18].

The present study is part of a comprehensive effort to fully characterize the changes in electrical properties of tissue with reversible and irreversible electroporation. This information should serve as feedback for real time control of the process of electroporation.

2. Materials and methods

A total number of 8 rats were randomly assigned into two different groups:

- Group "R": Reversible electroporation group (n=4); nominal electrical field=450 V/cm.
- Group "I": Irreversible electroporation group (n=4); nominal electrical field=1500 V/cm.

In both cases the liver was exposed *in vivo* and a sequence of 8 pulses of 100 μs duration and 100 ms period was applied through two flat circular electrodes separated at a distance of 5 mm. DC conductance was measured during the pulses and AC impedance was recorded in the inter-pulse intervals and for 30 min after the electroporation sequence. Resulting spectroscopic data were parameterized according to the Cole equation for a single dispersion.

Two hours and a half after the electroporation sequence, animals were euthanized and liver samples were prepared for histological analysis.

The following sections describe in more detail the employed materials, instruments and methods.

2.1. Apparatus

The general architecture of the system is shown in Fig. 1. The electroporation voltage pulses are applied to the sample through a pair of large annular electrodes, shown at the bottom left corner. These pulses are generated by a commercial pulse generator (ECM 830, *Harvard Apparatus*; Holliston, MA).

Passive electrical properties of the tissue are measured during and after the application of the electroporation pulse thanks to an automated switching scheme (this strategy has been employed previously by some researchers in the field [19,20]). After the electroporation pulse the impedance of the tissue between the electrodes is measured by using the four-electrode method in which the electroporation electrodes are used as the current injection electrodes and a pair of smaller inner electrodes are used to measure the induced voltage difference across the tissue sample. Recording of current and voltage during the electroporation pulse application is performed with a strategy similar to that described in Refs. [15,21,22]. Specific to our apparatus is the use of a small sensing resistor (1 Ω) for measurements instead of the use of a magnetic based current sensor. We choose to use a resistor rather than magnetic sensors because the sample impedances are expected to be much larger (>200 Ω) than in the previous studies and the error introduced by restive measurement becomes insignificant when taking into account the typical vertical resolution of oscilloscopes (8 bits).

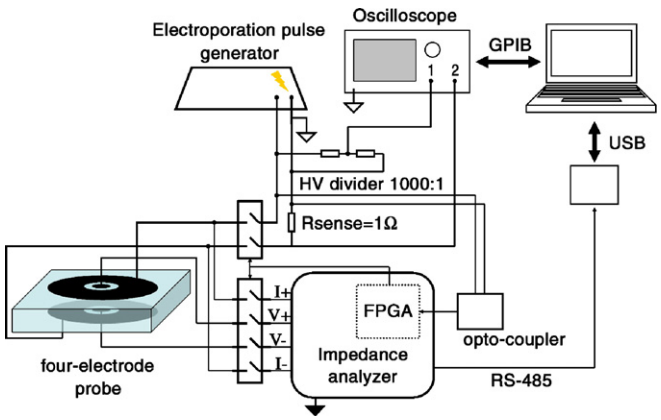

Fig. 1. General architecture of the developed system. The "quasi-DC" resistance is recorded by the oscilloscope during the electroporation pulses whereas AC impedance is measured afterwards.

2.1.1. Impedance analysis system

The post pulse impedance measurement is made with a custom developed impedance analyzer that is embedded in a single Printed Circuit Board (PCB) with the rest of components of the system. This subsystem is disconnected from the sample during the pulse application. Otherwise, the electronics would be damaged because of the high voltages applied for electroporation (up to 1500 V). As an alternative, we considered using surge protection mechanisms. However, such protection may have caused distortion of the impedance measurement or the electroporation fields.

Automatic connection and disconnection are performed by means of high-voltage reed relays with switch times below 2 ms (MS Series, Meder Electronic AG) that are controlled by a Field Programmable Gate Array (FPGA) that governs the whole system. Initially, the sample is connected to the electroporation pulse generator and disconnected from the AC impedance meter. After a high-voltage (HV) pulse signal is detected and a signal sent to FPGA through an optical-coupler, the system waits for a specified amount of time before connecting the impedance meter.

The impedance analyzer architecture (Fig. 2) is based on previous designs described in [23–25]. Briefly, an AC signal is

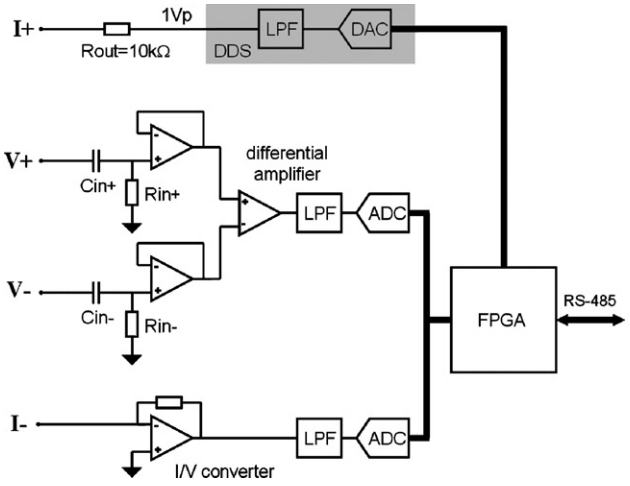

Fig. 2. Schematic representation of the fast impedance analyzer.

generated by using a Direct Digital Synthesizer (DDS) and injected into the sample through a limiting resistor (maximum current = 100 μA_p). Then, voltage difference and current signals are collected separately and processed to obtain their real and imaginary parts in relation to a reference signal. Basically, such processing is a digital cross-correlation between the input signals and the reference signal.

The system was configured to measure in the multi-frequency mode (1 kHz and 15.5 kHz) up to 500 ms after the end of last pulse. After this time point, frequency scans (ten frequencies from 1 kHz to 400 kHz) were recorded for 30 min.

2.1.2. Electrode setup

Fig. 1 shows the electrode setup in relation to the entire apparatus. It is used for both electroporation and impedance measurement. It consists of two parallel plates that clamp the liver lobe. Plates are separated 5 mm apart by spacers inserted in between them and the whole setup is held by clips. Mechanically it is equivalent to the setup used in Ref. [9].

Fig. 3 shows a schematic of the electrodes and their placement. The vertical left line in Fig. 3 is the line of symmetry and the figure shows half the plates. Each plate is made of a large external annular electrode (external diameter = 10 mm) for electroporation and current injection (I+, I−) and a smaller circular electrode (external diameter 1 mm) for voltage detection (V+, V−). Fig. 3 also shows a typical electrical field magnitude distribution during the experiments discussed later in this paper. For the reversible group, the voltage that was set across the electroporation electrodes was 225 V, which in the experiment were applied in eight 100 μs pulses separated by 100 ms. This voltage was chosen to produce an electrical field around 450 V/cm and it should produce reversible electroporation [7]. The calculations in the figure show that presence of the inner voltage measurement electrodes distorts the electric field during electroporation when compared to a two disk arrangement. However, as shown in the simulation depicted in Fig. 3, the "shadowed" tissue volume is not significant (<1% of electroporated volume).

The electroporation plates were produced by using standard Printed Circuit Board technology (Sierra Proto Express Inc., Sunnyvale, CA, USA). FR-4 was selected as the board material and soft bondable gold was selected as finishing for the electrodes.

In order to reduce the electrode-tissue interface impedance, platinum black was deposited with electrochemical deposition on the gold electrodes [26]. Such interface impedance reduction is useful for four-electrode impedance measurements [27]. Here, we have also found that it reduces the magnitude of the electrochemical DC voltage after the application of the HV pulses.

The cell constant, K, defined as the ratio between the resistivity and the measured resistance, will depend on the sample geometry. However, taking into account a range of reasonable expected geometries, finite-element simulations provide a value for $K = 2.76 \pm 0.05$ cm. Experimental measurements with saline solutions give a slightly larger value, $K = 2.9$ cm. The results are evaluated with $K = 2.8$ cm.

In the case that the external annular electrodes are used both for current injection and voltage drop reading, simulations provide a value for $K = 2.3$ cm. This is the cell constant value that we employ here to scale conductivity values during the electroporation pulses.

At this point it may be worth to note that four-electrode method is advisable, if not necessary, for small-signal impedance measurements in order to avoid the error introduced by the parasitic electrode-tissue interface impedance, particularly at low frequencies since it shows a capacitive behavior. On the other hand, at high voltages or current densities this impedance is minimized and becomes resistive rather than capacitive [26] since electrode transfer reactions can occur at the electrodes.

2.1.3. Data processing and representation

In an electrical component, electrical impedance at a specific frequency defines the mathematical relation between the applied alternating current and the resulting voltage between

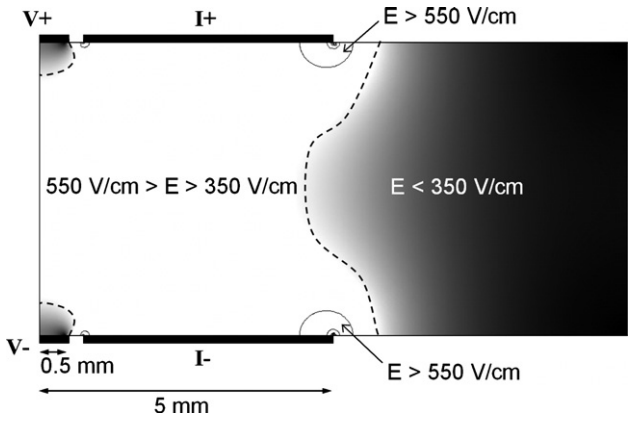

Fig. 3. Finite-element simulation (FEMLAB) of the electric field produced by the probe (axial symmetry). The selected electric field for reversible electroporation is 450 V/cm (225 V were applied between electrodes I+ and I−). At the electrode edges the field is higher and, presumably, irreversible electroporation or burning could be caused. Under electrodes V+ and V− a shadowed volume appears since current is shunted by these electrodes.

the component terminals. In addition to the relation of magnitudes between the voltage and the current ("impedance magnitude"), a relative time delay between both signals can also be observed that can be expressed in degrees ("impedance phase angle"; a phase angle of −90° means that the voltage signal is delayed with respect to the current signal by a quarter of the period). Therefore, for each frequency the impedance can be represented with two numerical values that are usually expressed as a complex number.

The simplistic cell model presented in the introduction, which consists of a resistance for the extra-cellular medium in parallel with a capacitance accounting for the cell membrane in series with a resistance representing the intra-cellular medium, was first proposed by Fricke and Morse in 1925 [28]. It represents one relaxation process with a single characteristic time constant and, in the frequency domain, corresponds to a single dispersion, that is, a transition between two frequency-independent levels (see Ref. [29] for more details about these concepts). However, since the first studies, it was observed that this capacitive model was not accurate enough to fit the experimental results in cell suspensions or living tissue studies. When the impedance values measured at multiple frequencies are represented in a Bode plot, it is observed that the behavior of the capacitive model is steeper than the results from actual bioimpedance data. Moreover, in the complex plane (imaginary part versus real part) both, the capacitive model and the experimental results, produce a semicircle but, in the case of the actual data the center is not on the real axis. This phenomenon is usually described as "depressed semicircles" and it is not only observed in living tissues but also in some composite materials [30].

In 1940 Keneth S. Cole [31] introduced the first mathematical expression able to fit the "depressed semicircles" found experimentally. It is known as the Cole equation and here we have employed it to characterize the impedance spectrogram obtained from multi-frequency measurements recorded before and after electroporation (Cole equation expressed here as in Ref. [29]):

$$\mathbf{Z} = R_\infty + \frac{\Delta R}{1 + (j\omega\tau)^\alpha}, \quad \Delta R = R_0 - R_\infty \tag{1}$$

where $\mathbf{Z}$ is the impedance value at frequency ω, j is the complex number $(-1)^{1/2}$, R_∞ is the impedance at infinite frequency, R_0 is the impedance at zero frequency, τ is the characteristic time constant and α is a dimensionless parameter with a value between 0 and 1.

In other words, for each time sample, the parameters R_∞, R_0, τ and α were adjusted to reproduce the actual impedance spectrogram. The fitting was automatically performed from the measurements at frequencies from 1 kHz to 65 kHz (8 points) with custom developed routines based on the fitting algorithm presented in Ref. [32]. Higher frequencies were not used for fitting since significant phase error due to parasitic capacitances was detected. As it can be observed in Fig. 6, Cole modeling produced reasonable good results.

After the fitting, the Cole parameters (R_∞, R_0, τ and α) were plotted (expressed as mean ± standard deviation). The R_∞ and R_0 parameters were scaled according to the probe cell constant (K=2.8 cm) and their values were expressed as resistivities (Ω cm) instead of resistances (Ω).

Quasi-DC conductance was computed at the end of the pulses from recorded current, $i(t)$, and voltage, $v(t)$, as $g(t)=i(t)/v(t)$. Then it was scaled by $1/K$ (1/2.3) in order to obtain the quasi-DC conductivity.

During the inter-pulse intervals and up to 500 ms after the electroporation sequence, impedance was only obtained at two frequencies. This is insufficient to generate a Cole approximation. However, since Cole modeling provided good results before electroporation and after the 500 ms time lag, we have considered that the pre-pulse Cole model is still valid during these intervals and that R_0 and τ are the only parameters that change significantly. This yields us to compute the value of R_0 as proportional to the impedance magnitude at 1 kHz, in particular:

$$R_0 = 1.03 \times |Z|_{1\ \mathrm{kHz}} \tag{2}$$

To obtain the 1.03 scaling factor we have averaged the ratio $R_0/|Z|_{1\ \mathrm{kHz}}$ for all Cole fittings obtained before and immediately after electroporation.

2.2. Animals and anesthesia

Male Sprague-Dawley rats (250–350 g) were obtained from Charles River Labs through the Office of Laboratory Animal Care at the University of California, Berkeley. They received humane care from a properly trained professional in compliance with both the Principals of Laboratory Animal Care and the Guide for the Care and Use of Laboratory Animals, prepared and formulated by the Institute of Laboratory Animal Resources and published by the U.S. National Institutes of Health (NIH).

The experiment started with anesthetization of the animal via intraperitoneal injection of Nembutal solution (50 mg/ml sodium pentobarbital, Abbott Labs, North Chicago, IL) for a total of 100 mg sodium pentobarbital per kg of rat. Thirty minutes later, the liver was exposed via midline incision. Then, one lobe of the liver was clamped between the two electrode plates at a separation of 5 mm, multi-frequency impedance was measured for 2 min and the corresponding sequence of square pulses was applied. After that, impedance was recorded for 30 min continuously. Finally, after 2 hours and a half, the animal was euthanized and liver samples of the area of interest were prepared for histology.

2.3. Histology

To fix the liver at its current state for microscopic viewing, we flushed the vasculature with physiological saline for 10 min at a hydrostatic pressure of 80 mmHg from an elevated IV drip. This was accomplished by injecting the fluid into the left ventricle and letting it exit from a cut made in the right atrium. Immediately following saline perfusion, a 5% formaldehyde fixative was perfused in the same way for 10 min. The treated liver lobe was then removed and stored in the same

formaldehyde solution. Hematoxylin–eosin staining was then performed on cross-sections through the center of the treated region to elucidate the morphology.

3. Results

3.1. Conductivity evolution during electroporation

As shown in the examples of Figs. 4 and 5, tissue conductivity increases during the electroporation sequence in the reversible and the irreversible cases. Specifically, taken into account pre-electroporation values and values immediately after the last pulse, there is an increase of conductivity equal to 9±3% in the reversible group and equal to 43±1% in the irreversible group.

It is interesting to note that the conductivity during the 100 μs pulses ("*in-pulse*" conductivity) is quite higher than the conductivity during the inter-pulse intervals, particularly in the irreversible group. Such *in-pulse* conductivity is reached immediately in the reversible group in terms of time resolution of the oscilloscope captured data (5 μs). On the other hand, in the irreversible group the *in-pulse* conductivity increases continuously during the pulse after an immediate initial step in conductivity. Unfortunately, electrical interference generated by the pulse generator made impossible to register waveforms suitable for graphical representation. Only individual samples could be assessed. In particular, in Figs. 4 and 5 the circles represent the *in-pulse* conductivity values at the end of the pulse.

It is also noticeable the fact that the in-pulse conductivity values saturate in the irreversible group whereas in the reversible group increase almost linearly with each pulse. Nevertheless, the inter-pulse conductivity increases in both cases after each pulse.

Phase angle measurement at 1 kHz during this stage does not produce significant results due to its low absolute value (~|−1|°). On the other hand, phase angle at 15.5 kHz gives similar information to that shown in Figs. 4 and 5. Mean value before electroporation is −18.7° and, because of electroporation, it increases 7.4±0.9° in the irreversible group and 2.2±0.9° in the reversible group.

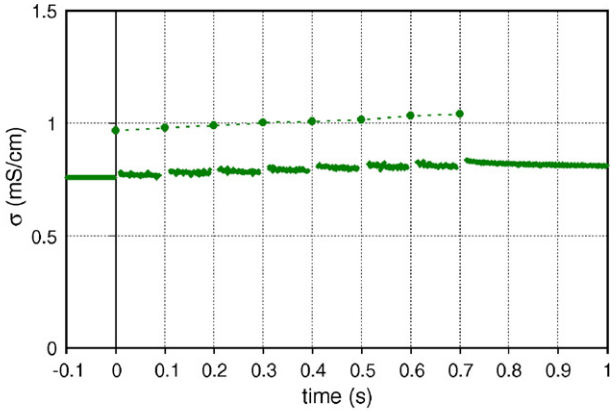

Fig. 4. Conductivity evolution during the electroporation sequence in an example from the reversible group (8 pulses of 100 μs and 450 V/cm). Points marked with circles and joined with a dashed line represent the quasi-DC conductivity obtained at the end of each electroporation pulse.

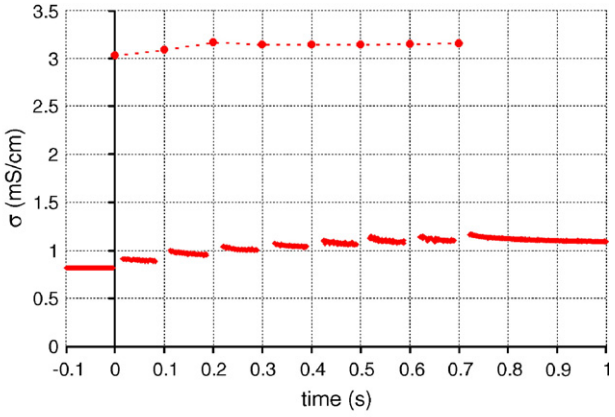

Fig. 5. Conductivity evolution during the electroporation sequence in an example from the irreversible group (8 pulses of 100 μs and 1500 V/cm). Points marked with circles and joined with a dashed line represent the quasi-DC conductivity obtained at the end of each electroporation pulse.

3.2. AC impedance after electroporation

As it can be observed in the example depicted in Fig. 6, Cole model fits reasonably well actual data before electroporation. After the high voltage pulse sequence, all Cole parameters, except R_∞, change significantly across time (Figs. 7–10) but the single dispersion model is still valid. That is, actual data can be approximated by a single semicircle in the impedance locus plot.

Figs. 7 and 8 show an interesting phenomenon related to the reversible group: after the expected initial drop of DC resistivity ($=R_0=\rho=1/\sigma$) caused by electroporation (Fig. 4), R_0 starts to increase, surpasses its original values before electroporation and reaches a peak at about 100 s after electroporation. After that, R_0 slowly decreases to a value slightly below its original value.

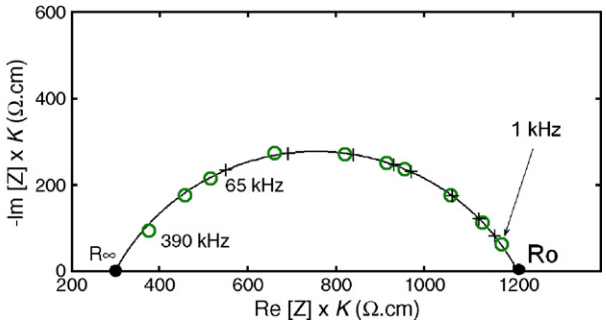

Fig. 6. Example of impedance locus (imaginary part of impedance, Im [Z], versus real part of impedance, Re [Z]) before electroporation. Circles denote actual data and the continuous line and crosses denote the corresponding Cole model. Measured impedance values and Cole parameters are scaled according to the probe cell constant (K=2.8 cm) in order to provide cell geometry independent values, that is, they are scaled for the reference measurement cell (section=1 cm^2, length=1 cm).

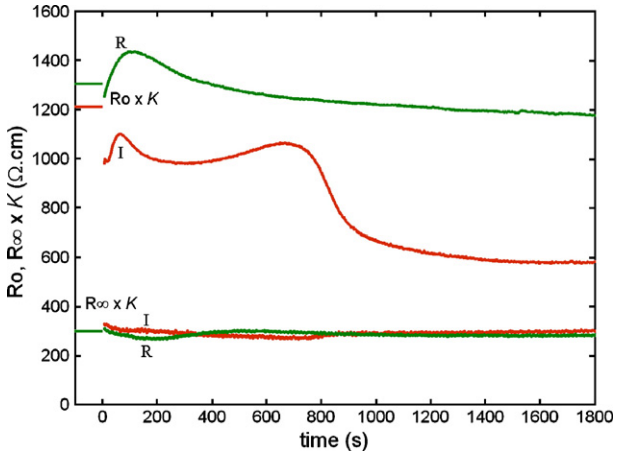

Fig. 7. Examples of evolution of Cole parameters R_0 and R_∞ from the reversible (R) and the irreversible (I) groups after electroporation (time=0). Values are scaled according to the probe cell constant (K=2.8 cm).

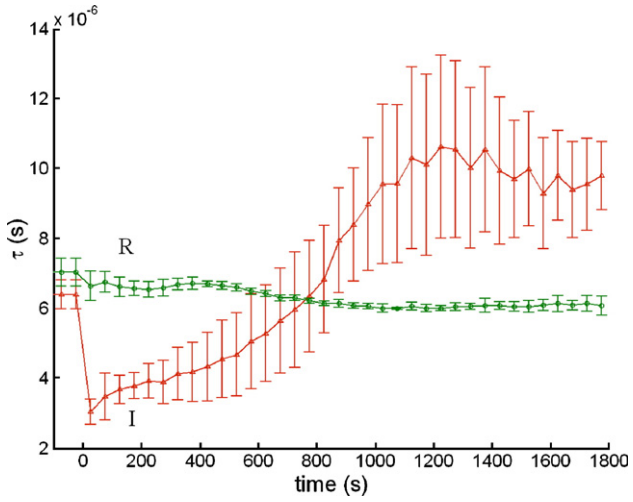

Fig. 9. Evolution of mean value of Cole parameter τ in the reversible (R) and the irreversible (I) groups after electroporation (time=0). Error bars represent ±standard deviation.

The irreversible group also shows a peak in resistivity after the initial drop caused by electroporation. However, in this case, after-electroporation values are significantly lower than the original ones. Moreover, at about 12 min after this first resistivity drop due to electroporation there is a second step decrease.

The time constant (τ) also distinguishes both groups markedly after electroporation (Fig. 9). Quite interestingly, the α parameter is not significantly different between both groups just after electroporation (Fig. 10). Nevertheless, after 30 min it is the parameter that produces most significant differences between both groups.

3.3. Macroscopic and microscopic observations

Naked-eye observation of electroporated livers after saline perfusion yields very different results for both groups: irreversibly electroporated livers show a very distinctive dark red circular area at the location of the electrodes whereas livers from reversible group have no sign except an occasional, slight and thin reddening where the electrode edges were placed.

Presumably, the distinctive dark reddening of irreversibly electroporated livers is due to the accumulation of red blood cells (RBC) that can be microscopically observed (Fig. 11) [9]. Such entrapping of RBCs could to be related to the observed destruction of endothelial structures of the liver vasculature system.

Besides the pooling of RBCs and the destruction of endothelial structures, microscopy (Fig. 11) also shows a very significant increase of the inter-hepatocyte space that seems to be caused by massive cell lysis.

Microscopy of reversibly electroporated areas shows that the hepatocytes appear intact, with intact cell membranes and distinct clear nuclei. Some of the hepatocytes give the impression to be divided or to be in the process of division.

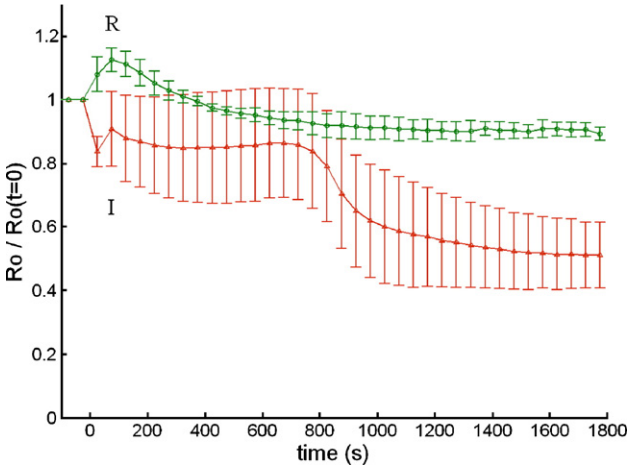

Fig. 8. Evolution of mean value of Cole parameter R_0 in the reversible (R) and the irreversible (I) groups after electroporation (time=0). Error bars represent ±standard deviation. R_∞ is not displayed since its time variation is much lower than the standard deviation.

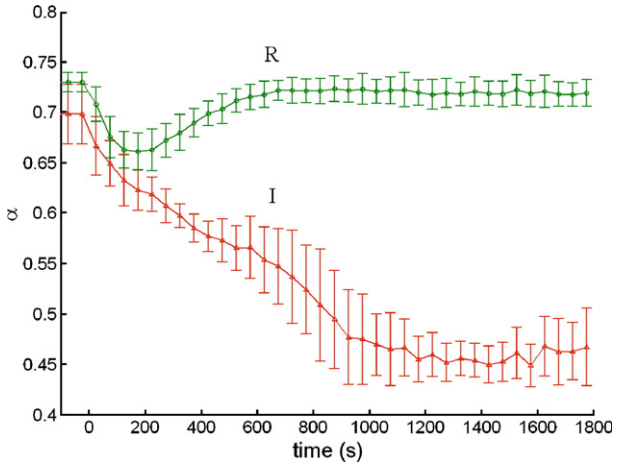

Fig. 10. Evolution of mean value of Cole parameter α in the reversible (R) and the irreversible (I) groups after electroporation (time=0). Error bars represent ±standard deviation.

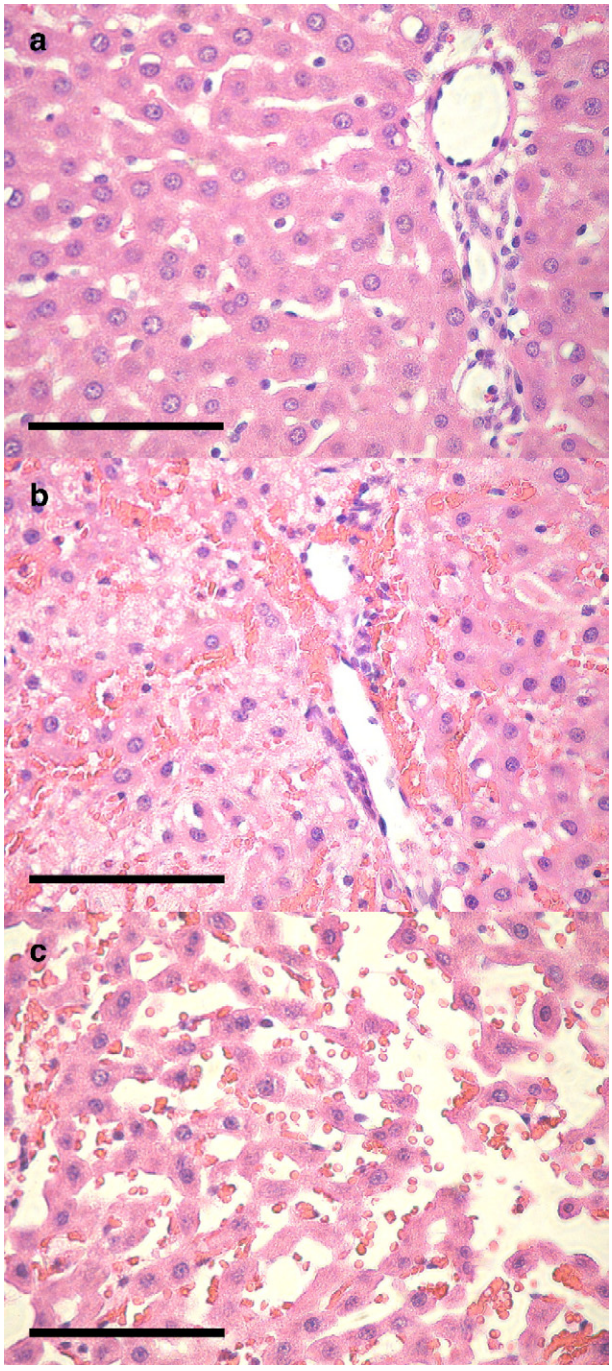

Fig. 11. Microscopic pictures of electroporated livers. (a) Portal vein branch, hepatic artery branch and bile duct in an area of a reversibly electroporated liver where electrical fields are below 300 V/cm; intact hepatocytes and some damage to endothelial cells. (b) Presumably location of portal vein and hepatic artery branches in a treated area of an irreversibly electroporated liver; very significant entrapping of RBCs into the hepatic sinusoids, destruction of endothelial structures. (c) Another treated area of an irreversibly electroporated liver; significantly increased inter-hepatocyte spaces and loss of cell membrane integrity. Bars indicate 100 μm.

On the other hand there are several sites in which the endothelial cells appear to have become detached from the blood vessels walls. At other sites the endothelial cells are intact.

In contrast, at irreversibly electroporated areas (Fig. 11b), hepatocyte membrane integrity is not clear and nuclei are mostly pyknotic. In addition, RBCs are trapped inside the sinusoids and there is hemorrhage near the large blood vessels. Similarly to results presented in [9], the larger blood vessels have retained their structure and are devoid of debris. At some sites in the irreversible electroporated area (Fig 11c) the damage to the cell membrane is profound and the cells have completely lost integrity.

4. Discussion

As expected, tissue conductivity increases during the electroporation pulse sequence due to cell membrane "shunting" and it tends to slowly recover its original value afterwards, presumably because of membrane resealing (Figs. 4 and 5). Such recovery can be approximated by an exponential function with a time constant of the order of 0.1 s.

In the case of reversible electroporation, passive electrical properties almost recover their original values 15 min after electroporation. In fact, the slight differences could be attributed to irreversible electroporation of localized portions of tissue due to nonuniform electric fields caused by edge effects at the electrodes (Fig. 3.). Therefore, impedance seems to confirm that tissue properties are only temporarily affected by electroporation if certain electrical field thresholds are not surpassed.

It is more interesting, however, the unexpected stage of increased resistivity after electroporation (Figs. 7 and 8). Since it occurs within the time scale in which reversible blood occlusion is manifested after electroporation [33] it is reasonable to think that both phenomena are linked. A possible explanation could be based on the fact that ischemia (i.e. blood occlusion) induces cell swelling and, consequent, narrowed extra-cellular paths for low-frequency currents [25]. This type of behavior was found at low frequencies in liver in response to artificial ischemia ($\Delta|Z| > 10\%$ in 1 min) [34]. Therefore, although membrane conductivity would be increased due to electroporation, overall conductivity would be reduced because of narrowed extra-cellular paths due to ischemia.

Short term (minutes) perfusion impediment after electroporation has been described as being the result of reflex constriction of afferent arterioles [33]. For longer times, occlusion could be related to the direct effect of pulses on vascular endothelial cells. In this case, permeabilization of vasculature would lead to increased interstitial pressure and decreased intravascular pressure which would finally yield to occlusion. As explained in Ref. [35] for intestinal epithelial monolayers, different causes can be argued to explain an increase of endothelial permeability due to electroporation: a) opening of tight junctions due to cytoskeleton alteration; b) transcellular transport through reversible electropores; and c) direct transport through holes left by killed cells.

Another plausible explanation for the stage of increased resistivity after electroporation could be based on the fact that electroporation increases cell membrane permeability to water and, consequently, induces cell swelling due to unbalanced osmotic pressure. Such explanation was proposed by Abidor et al. to interpret a similar observation in the case of cell pellets [36], which are simple cells aggregates obtained through centrifugation

and obviously do not have blood vessels and do not experience systemic response to electroporation. Both explanations are feasible and it is possible that they occur simultaneously.

Fig. 12 shows clearly that three distinctive regions can be identified in the evolution of R_0 after the reversible electroporation sequence. Up to 10 s after electroporation the response is compatible with the exponential response observed in Fig. 4. Thus, we hypothesize that such evolution is dominated by membrane resealing. After that, the slope increases significantly, indicating that another phenomenon is active. In this case, as it has been already pointed out, we suggest that the dominant process may be blood occlusion. Finally, we attribute the resistivity decrease to cessation of the occlusion mechanism ("deocclusion"). Hence we are assuming that the blood occlusion mechanism is reversible in this case.

Irreversible effects on tissue are noticeable both in histology and impedance characterization. Low R_0 values 30 min after electroporation are probably caused by the enlargement of inter-hepatocyte spaces that can be observed in histological samples (Fig. 11c) and that is presumably caused by cell destruction. However, permanent cell membrane permeabilization or cell fusion could also explain such result.

In Fig. 12 the number of distinctive regions for the irreversible case is six. As in the reversible case, we attribute the first one to the membrane resealing process. Unfortunately, we are not able to satisfactorily explain the second region in which R_0 decreases slightly. The third and fourth regions are similar in slope to the second and third regions in the reversible case. Moreover, they occur in the same time range. Thus, we hypothesize that they are dominated by the reversible blood occlusion mechanism. In order to explain the last two regions we make use of the histological observations. We suggest that entrapping of RBCs into the hepatic sinusoids (Fig 11b) after blood flow resumes may explain the increase of R_0 observed in the fifth region. That is, the accumulation of RBCs in the sinusoids would narrow the extra-cellular paths for low-frequency currents and that would lead to R_0 increase. Finally, the observed enlargement of inter-hepatocyte spaces and the loss of membrane integrity would explain the last region in which resistivity decreases dramatically. Such abrupt decrease could be the result of the superposition of opposite mechanisms. That is, progressive cell lysis would be happening progressively since the electroporation sequence but it would be "hidden" by processes that tend to increase R_0, then, after those processes finish, resistivity decrease would be manifested abruptly. The fact that τ and α parameters change progressively after electroporation and that they do not show any abrupt change seems to reinforce the hypothesis of the superposition of processes.

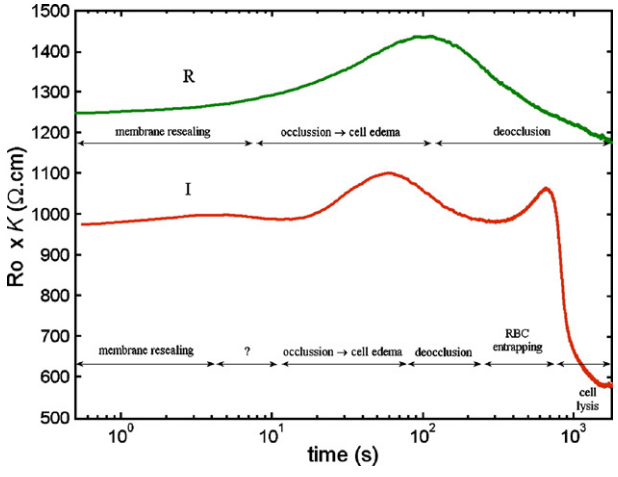

Fig. 12. Examples of evolution of Cole parameter R_0 depicted with logarithmic time scale (same examples than in Fig. 7). For different regions we have hypothesized a dominant process. The origin of the time scale ($t=0$) is at the end of the electroporation pulse sequence. Values are scaled according to the probe cell constant ($K=2.8$ cm).

R_∞ represents the impedance at infinite frequency. At high frequencies (>10 MHz) cell membranes are not an impediment for currents and they become "invisible" in terms of impedance. Therefore it was expected that R_∞ would not to show significant changes because of electroporation. Only combined extra-cellular and intra-cellular conductivity changes would have produced R_∞ changes. As a matter of fact, the slight decrease of R_∞ at about 3 min after electroporation in the reversible group in Fig. 7 could be explained as being the result of metabolic by-products accumulation caused by occlusion. That is, this observation would reinforce the blood occlusion hypothesis. Nevertheless, despite this phenomenon was repetitively observed in the four animals, it is advisable not to extract this sort of conclusions from R_∞ since it does not change significantly and the associated error could be quite important (note that higher frequencies are not considered for Cole fitting due to detected phase angle error).

Cole model parameters τ and α are more difficult to interpret in biophysical terms than R_0 and R_∞. Some researchers derive an equivalent capacitance from the time constant (τ) and the cell model described in the introduction in order to understand the behavior of the membranes. However such procedure would only be valid in the case that $\alpha=1$.

The α parameter is even more cryptic. There is no general agreement on the physical meaning of this parameter. Most authors suggest that it is related to the heterogeneity of cell sizes and shapes in living tissues. However, it is difficult to fit such explanation to experimental results such as those presented here in which α decreases significantly and an increase of cell size heterogeneity is not observed. On the other hand, current results and observations seem to reinforce the idea that α is strongly related to the morphology of the extra-cellular spaces [37].

5. Conclusion

From the results presented here it can be concluded that impedance measurements can be employed to detect and distinguish reversible and irreversible electroporation in *in vivo* and *in situ* liver tissue. Although multi-frequency measurements provide interesting information for characterization purposes, single-frequency measurements will be sufficient for practical purposes. Both, impedance magnitude at low frequencies and impedance phase angle at intermediate frequencies (from 10 kHz to 100 kHz) should produce reliable immediate assessment of the electroporation outcome.

Nevertheless, if it is required to avoid distortion from blood occlusion effects, measurements should be taken immediately after the electroporation sequence, ideally in tenths of second. On the other hand, later impedance measurements can be employed to follow up the blood occlusion phenomenon and to confirm destruction of tissue due to irreversible electroporation.

Finally, it must be noted that not only the impedance during the inter-pulse intervals or immediately after the whole electroporation sequence is useful to distinguish between reversible and irreversible electroporation but also the in-pulse conductivity can be employed for such a purpose.

Acknowledgements

This work was supported in part by the U.S. National Institutes of Health (NIH) under Grant NIH R01 RR018961. We thank Liana Horowitz for performing the animal experiment reported in this study. BR has a financial interest in Excelling Life Sciences and Oncobionic which are companies in the field of Electrical Impedance Tomography of electroporation and irreversible electroporation, respectively.

References

[1] E. Neumann, M. Schaeffer-Ridder, Y. Wang, P.H. Hofschneider, Gene transfer into mouse lymphoma cells by electroporation in high electric fields, EMBO J. 1 (1982) 841–845.
[2] L.M. Mir, Therapeutic perspectives of in vivo cell electropermeabilization, Bioelectrochemistry 53 (2001) 1–10.
[3] M.J. Jaroszeski, R. Heller, R. Gilbert, Electrochemotherapy, Electrogenetherapy, and Transdermal Drug Delivery: Electrically Mediated Delivery of Molecules to Cells, Humana Press, Totowa, New Jersey, 2000.
[4] D.A. Dean, Nonviral gene transfer to skeletal, smooth, and cardiac muscle in living animals, Am. J. Physiol., Cell Physiol. 289 (2005) C233–C245.
[5] L.M. Mir, P.H. Moller, F. Andre, J. Gehl, Advances in Genetics, Academic Press, 2005, pp. 83–114.
[6] A. Gothelf, L.M. Mir, J. Gehl, Electrochemotherapy: results of cancer treatment using enhanced delivery of bleomycin by electroporation, Cancer Treat. Rev. 29 (2003) 371–387.
[7] R.V. Davalos, L.M. Mir, B. Rubinsky, Tissue ablation with irreversible electroporation, Ann. Biomed. Eng. 33 (2005) 223.
[8] L. Miller, J. Leor, B. Rubinsky, Cancer cells ablation with irreversible electroporation, Technol. Cancer Res. Treat. 4 (2005) 699–706.
[9] J. Edd, L. Horowitz, R.V. Davalos, L.M. Mir, B. Rubinsky, In-vivo results of a new focal tissue ablation technique: irreversible electroporation, IEEE Trans. Biomed. Eng. 53 (2006) 1409–1415.
[10] U. Cegovnik, S. Novakovic, Setting optimal parameters for in vitro electrotransfection of B16F1, SA1, LPB, SCK, L929 and CHO cells using predefined exponentially decaying electric pulses, Bioelectrochemistry 62 (2004) 73–82.
[11] G. Pucihar, T. Kotnik, M. Kanduser, D. Miklavcic, The influence of medium conductivity on electropermeabilization and survival of cells in vitro, Bioelectrochemistry 54 (2001) 107–115.
[12] M. Puc, S. Corovic, K. Flisar, M. Petkovsek, J. Nastran, D. Miklavcic, Techniques of signal generation required for electropermeabilization. Survey of electropermeabilization devices, Bioelectrochemistry 64 (2004) 113–124.
[13] Y. Huang, B. Rubinsky, Micro-electroporation: improving the efficiency and understanding of electrical permeabilization of cells, Biomed. Microdevices 3 (1999) 145–150.
[14] B. Rubinsky, Y. Huang, Controlled electroporation and mass transfer across cell membranes, US patent 6300108, 2001.
[15] M. Pavlin, M. Kanduser, M. Rebersek, G. Pucihar, F.X. Hart, R. Magjarevic, D. Miklavcic, Effect of cell electroporation on the conductivity of a cell suspension, Biophys. J. 88 (2005) 4378–4390.
[16] S.B. Dev, D. Dhar, W. Krassowska, Electric field of a six-needle array electrode used in drug and DNA delivery in vivo: analytical versus numerical solution, IEEE Trans. Biomed. Eng. 50 (2003) 1296.
[17] B. Rubinsky, Y. Huang, Electrical Impedance Tomography to control electroporation, US patent 6,387,671, 2002.
[18] R.V. Davalos, B. Rubinsky, D.M. Otten, A feasibility study for electrical impedance tomography as a means to monitor tissue electroporation for molecular medicine, IEEE Trans. Biomed. Eng. 49 (2002) 400–403.
[19] K.J. Kinosita, T.Y. Tsong, Voltage-induced conductance in human erythrocyte membranes, Biochim. Biophys. Acta 554 (1979) 479–497.
[20] I.G. Abidor, L.H. Li, S.W. Hui, Studies of cell pellets: I. Electrical properties and porosity, Biophys. J. 67 (1994) 418–426.
[21] L.F. Cima, L.M. Mir, Macroscopic characterization of cell electroporation in biological tissue based on electrical measurements, Appl. Phys. Lett. 85 (2004) 4520–4522.
[22] U. Pliquett, R. Elez, A. Piiper, E. Neumann, Electroporation of subcutaneous mouse tumors by trapezium high voltage pulses, Bioelectrochemistry 62 (2004) 83–93.
[23] A. Ivorra, Contributions to the Measurement of Electrical Impedance for Living Tissue Ischemia Injury Monitoring, Electronic Eng. Dept., Universitat Politècnica de Catalunya, Barcelona, 2005.
[24] T. Dudykevych, E. Gersing, F. Thiel, G. Hellige, Impedance analyser module for EIT and spectroscopy using undersampling, Physiol. Meas. 22 (2001) 19–24.
[25] B. Rigaud, J.P. Morucci, N. Chauveau, Bioelectrical impedance techniques in medicine. Part I: bioimpedance measurement. Second section: impedance spectrometry, Crit. Rev. Biomed. Eng. 24 (1996) 257–351.
[26] L.A. Geddes, Electrodes and the Measurement of Bioelectric Events, Wiley-Interscience, New York, 1972.
[27] A. Ivorra, Contributions to the Measurement of Electrical Impedance for Living Tissue Ischemia Injury Monitoring, Electronic Eng. Dept., Universitat Politècnica de Catalunya, Barcelona, 2004.
[28] K.S. Cole, Membranes, Ions and Impulses, University of California Press, Berkeley, 1972.
[29] S. Grimnes, O.G. Martinsen, Bioimpedance and Bioelectricity Basics, Academic Press, London, UK, 2000.
[30] J.R. MacDonald, Impedance Spectroscopy: Emphasizing Solid Materials and Systems, John Wiley and Sons, New York, 1987.
[31] K.S. Cole, Sympos Quant Biol, Cold Spring 1940, pp. 110–122.
[32] O. Casas, Contribución a la obtención de imágenes paramétricas en tomografía de impedancia eléctrica para la caracterización de tejidos biológicos, Universitat Politècnica de Catalunya, Barcelona, 1998.
[33] J. Gehl, T. Skovsgaard, L.M. Mir, Vascular reactions to in vivo electroporation: characterization and consequences for drug and gene delivery, Biochim. Biophys. Acta 1569 (2002) 51–58.
[34] D. Haemmerich, O.R. Ozkan, J.Z. Tsai, S.T. Staelin, S. Tungjitkusolmun, D.M. Mahvi, J.G. Webster, Changes in electrical resistivity of swine liver after occlusion and postmortem, Med. Biol. Eng. Comput. 40 (2002) 29–33.
[35] E.B. Ghartey-Tagoe, J.S. Morgan, A.S. Neish, M.R. Prausnitz, Increased permeability of intestinal epithelial monolayers mediated by electroporation, J. Control. Release 103 (2005) 177–190.
[36] I.G. Abidor, L.H. Li, S.W. Hui, Studies of cell pellets: II. Osmotic properties, electroporation, and related phenomena: membrane interactions, Biophys. J. 67 (1994) 427–435.
[37] A. Ivorra, M. Genesca, A. Sola, L. Palacios, R. Villa, G. Hotter, J. Aguilo, Bioimpedance dispersion width as a parameter to monitor living tissues, Physiol. Meas. 26 (2005) S165–S173.